Chemical Science

Accepted Manuscript

This article can be cited before page numbers have been issued, to do this please use: G. Han, C. M. Collins, M. Sonni, L. M. Daniels, A. Vasylenko, R. Chen, C. Robertson, M. S. Dyer, J. B. Claridge and M. J. Rosseinsky, *Chem. Sci.*, 2026, DOI: 10.1039/D5SC09834C.

ROYAL SOCIETY OF CHEMISTRY

rsc.li/chemical-science

Superionic Lithium Mobility in Low Symmetry $Li_7Si_2S_7I$ Polymorph Accessed via Si_2S_7 Dimer Reorientation

Guopeng Han,[a] Chris M. Collins,[a,b] Manel Sonni,[a] Luke M. Daniels,[a] Andrij Vasylenko,[a] Ruiyong Chen,[a] Craig M. Robertson,[a] Matthew S. Dyer,[a,b] John B. Claridge,[a,b] and Matthew J. Rosseinsky*[a,b]

[a] Department of Chemistry, University of Liverpool, Crown Street, Liverpool, L69 7ZD, United Kingdom

[b] Leverhulme Research Centre for Functional Materials Design, Materials Innovation Factory, University of Liverpool, 51 Oxford Street, Liverpool, L7 3NY, United Kingdom

* Corresponding Author: M.J.Rosseinsky@liverpool.ac.uk

Abstract

We report the experimental discovery of $Li_7Si_2S_7I_{0.89}Cl_{0.11}$, a triclinic ($P\bar{1}$) analogue of the recently discovered monoclinic ($P2_1/n$) $Li_7Si_2S_7I$ (LSSI), which retains the high computationally predicted Li^+ ion conductivity of LSSI. $Li_7Si_2S_7I_{0.89}Cl_{0.11}$, which is effectively a polymorph of LSSI, maintains the same ordered anion packing based on the packing of spheres in NiZr intermetallic, however demonstrates a distinct ordering of the Si^{4+} framework-forming cations. While both structures feature Si_2S_7 dimers within hexagonal close-packed (hcp) anion motifs, their different arrangement in the triclinic material results in the alternating stacking of silicon-free and silicon-rich layers. $Li_7Si_2S_7I_{0.89}Cl_{0.11}$ has an additional Li^+ position compared to LSSI, sixteen in total, which maintains the large number of redundant low energy pathways favourable for superionic conduction. Thus, $Li_7Si_2S_7I_{0.89}Cl_{0.11}$ has a predicted ionic conductivity of 0.019(7) S cm^{-1} derived from molecular dynamics simulation of the experimentally measured structure and theoretical activation energy for bulk Li^+ ion transport of 0.16(4) eV, within error of those of monoclinic LSSI. These results demonstrate the structural resilience of the ordered S^{2-}/I^- anion net to changes in cation positions and crystal system, further exemplifying the ability of the net to afford diverse low barrier Li ion transport pathways and thus generate a predicted superionic conductivity. Polymorphism is generally thought to have a profound impact on ion transport, however the computational results here suggest that there are privileged anion frameworks with an intrinsic robustness to changes in cation distribution where superionic transport can persist.

Introduction

Solid-state electrolytes have gained significant attention as a safer and potentially higher-performance alternative to liquid electrolytes in next-generation battery technologies.[1-5] The minimisation of Li^+ coordination changes along the ion conduction pathway within the structure, particularly site energy equivalency provided by similar tetrahedral environments to reduce barriers for transport, is proposed as critical to achieving high Li^+ ion conductivity in the solid state.[6-8] This understanding is applied to the few established state-of-the-art solid

View Article Online
DOI: 10.1039/D5SC09834C

electrolytes that exhibit superionic (>10^{-2} S cm^{-1}) Li^+ conductivities comparable with that of liquid electrolytes, such as $Li_{10}GeP_2S_{12}$ (LGPS)[9] type materials,[10, 11] $Li_7P_3S_{11}$,[12, 13] and argyrodites.[14, 15] Recently, the superionic conductor $Li_7Si_2S_7I$ (LSSI) which represents a new structural family was discovered using a workflow integrating machine learning and structure prediction.[16] In contrast to the well-established LGPS and argyrodite structures, LSSI possesses a unique anion packing based on that of the intermetallic NiZr but with a distinct decoration pattern. This ordered S/I array creates a diverse range of interstitial sites available for cation occupation, and offers a wide range of lithium-ion pathways with low energy barriers that enable rapid lithium-ion conduction resulting in a high room temperature ionic conductivity of 1.01(4) × 10^{-2} S cm^{-1}. Subsequent substitutional optimisation of LSSI ($Li_7Si_{2-x}Ge_xS_7I$ where $x \leq 1.2$) further enhanced the Li^+ site disorder.[17] This isovalent substitution offers control over the Li^+ environment size and stabilizes the property-determining disorder to low temperature, yielding enhanced Li^+ transport in highly substituted (x = 1.0-1.2) materials that is comparable to the best solid-state electrolytes. The combination of multiple anions in the structure of LSSI provides additional scope for substitutional optimisation that extends beyond the cations, a well-established method for property control in both argyrodite and LGPS-type materials.[10, 11, 15, 18-20] Thus, LSSI presents a platform for explorative substitutional chemistry directed towards further performance enhancement similar to the initial discoveries of argyrodite and LGPS, and their subsequent compositional optimisation to yield the current state-of-the-art materials such as $Li_{6.6}Si_{0.6}Sb_{0.4}S_5I$ and $Li_{9.54}[Si_{0.6}Ge_{0.4}]_{1.74}P_{1.44}S_{11.1}Br_{0.3}O_{0.6}$.[10, 21]

In this study, we explore the substitution of I^- for Cl^- and discover triclinic ($P\bar{1}$) $Li_7Si_2S_7I_{0.89}Cl_{0.11}$, a polymorph of monoclinic ($P2_1/n$) $Li_7Si_2S_7I$, under specific crystal growth conditions. Sub-solidus investigation into the solid solution of $Li_7Si_2S_7I_{1-x}Cl_x$ revealed that only slight substitution of I^- for Cl^- is possible in the monoclinic $P2_1/n$ form of LSSI. The structure of triclinic $Li_7Si_2S_7I_{0.89}Cl_{0.11}$ is solved by single crystal X-ray diffraction, revealing an ordering of the framework-forming Si_2S_7 dimers that is distinct from LSSI. Theoretical assessment of ionic conductivity via *ab initio* molecular dynamics (AIMD) simulations demonstrates that $Li_7Si_2S_7I_{0.89}Cl_{0.11}$ retains superionic mobility despite the reduction in symmetry and changes to framework-forming cation positions.

Results and discussion

The direct substitution of I^- for Cl^- in $Li_7Si_2S_7I_{1-x}Cl_x$ is explored via single crystal growth procedures which utilised a range of LiCl-LiI eutectic fluxes (Supporting Information). Crystal growth with a 1:1 molar ratio of Li_2S and SiS_2 at 773 K in a 35%LiCl-65%LiI flux within a vacuum-sealed silica ampoule afforded a mixture of LiCl, LiI, and Li_2SiS_3, including single crystals shown by SEM-EDX to contain both iodine and chlorine, with compositional analysis of multiple crystals affording the composition $Si_{2.16(13)}S_{6.97(11)}I_{0.83(16)}Cl_{0.2(1)}$ (Figure S1). Single crystal X-ray diffraction demonstrates that these chloride-containing crystals adopt a different structure

View Article Online
DOI: 10.1039/D5SC09834C

from LSSI in the triclinic $P\bar{1}$ space group. The $P\bar{1}$ symmetry is retained over the temperature range 100-300 K (Supporting Information, Tables S2-5). The triclinic structure shares the same anion packing as monoclinic LSSI. Refinement reveals reduced electron density on the iodide site, in contrast to the full occupancy found in LSSI itself, consistent with substitution of the chloride indicated by SEM-EDX at that site, leading to a refined composition of $Li_7Si_2S_7I_{0.8873(17)}Cl_{0.1127(17)}$.

The packing of the S^{2-} and I^-/Cl^- in triclinic $Li_7Si_2S_7I_{0.89}Cl_{0.11}$ is based on the $3^3.4^2$ semiregular net observed in the binary intermetallic NiZr (Figure 1a). These anion layers stack in an ABAB sequence, generating the same alternating combination of hexagonal close-packed (hcp) and sheared face-centered cubic (fcc)-like anion motifs as observed in monoclinic LSSI (Figure 1), which define a diverse array of interstitial sites available for cation occupancy in triclinic $Li_7Si_2S_7I_{0.89}Cl_{0.11}$. The two Si^{4+} cations do not coordinate to the halide site and occupy adjacent tetrahedral 2*i* sites within the hcp motifs that are solely coordinated by the higher charged S^{2-} to form Si_2S_7 dimers. This motif is maintained from the structure of monoclinic LSSI, however, the locations of the framework forming Si^{4+} cations within the hcp fragment of the structures are different in the two symmetries. In triclinic $Li_7Si_2S_7I_{0.89}Cl_{0.11}$, the neighbouring Si_2S_7 dimers in each anion layer are uniformly oriented occupying the T^- sites (Figure 1c). This is in contrast to the two opposite orientations of Si_2S_7 dimers in the monoclinic structure (Figure 1d) which alternate along the *a* direction between T^+ and T^- tetrahedral environments *i.e.,* with the Si–S vector to the apex of the tetrahedron alternating in orientation. This distinct Si_2S_7 dimer arrangement in the structure of $Li_7Si_2S_7I_{0.89}Cl_{0.11}$ results in alternating Si^{4+}-free and Si^{4+}-rich layers stacked along *b* (Figure 1e), whereas the Si_2S_7 dimers are distributed evenly in the layers along *b* in monoclinic LSSI (Figure 1f).

View Article Online
DOI: 10.1039/D5SC09834C

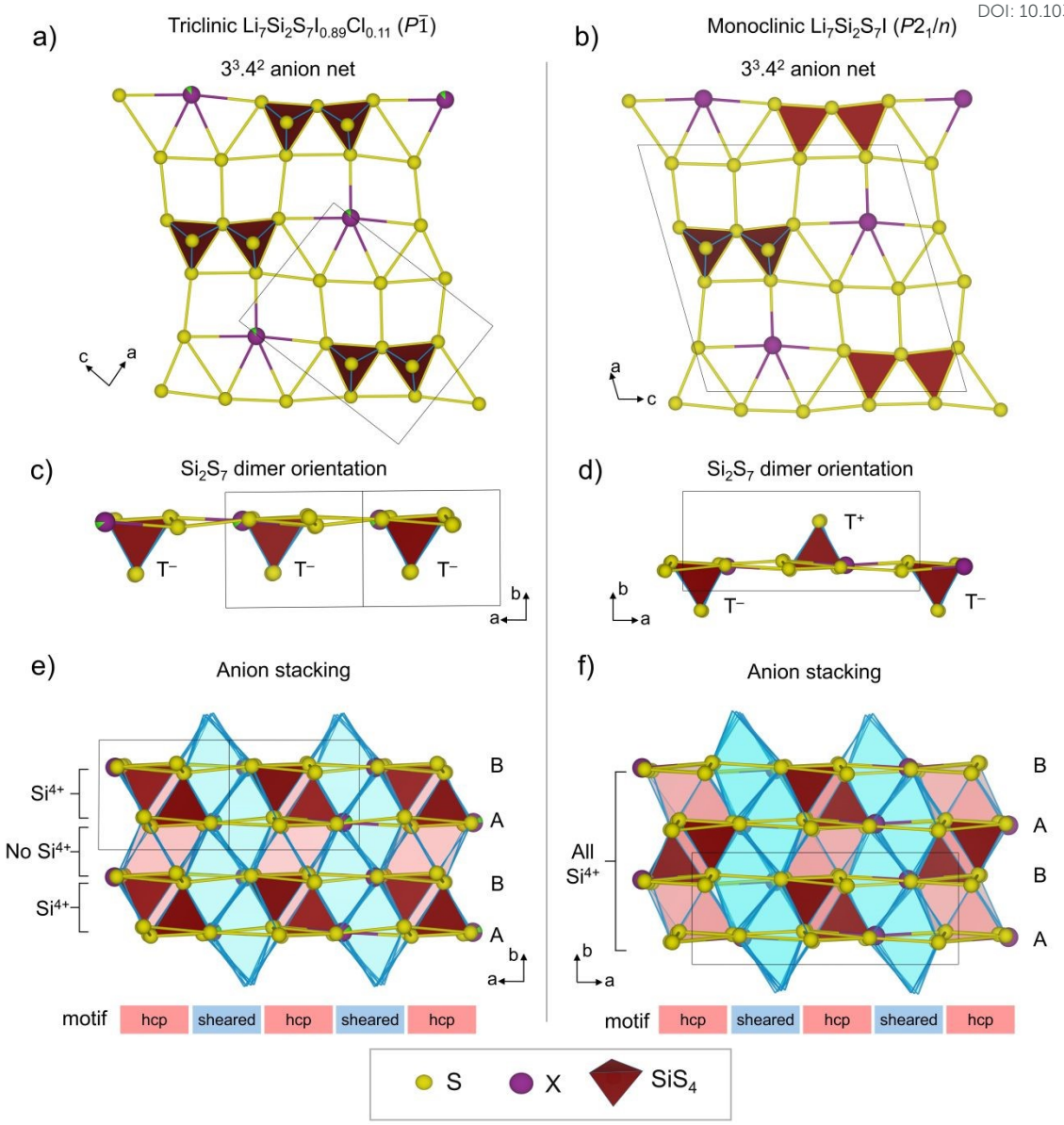

Figure 1. Comparison of anion packing, Si_2S_7 dimer arrangement and orientation in triclinic $Li_7Si_2S_7I_{0.89}Cl_{0.11}$ and monoclinic $Li_7Si_2S_7I$. In both a) $Li_7Si_2S_7I_{0.89}Cl_{0.11}$ and b) $Li_7Si_2S_7I$, the S^{2-} (yellow) and X^- (purple) anions are ordered in $3^3.4^2$ nets, which stack in an ABAB sequence along *b* to generate hcp (red shading) and sheared fcc-like (blue shading) motifs along the *a* direction shown in e) and f). The hcp motifs in both materials accommodate the Si_2S_7 tetrahedral dimers (brown) which are arranged on the net in the same way but are oriented differently. In $Li_7Si_2S_7I_{0.89}Cl_{0.11}$ the dimers orient c) below the plane of the anion net (T^- tetrahedral environments), compared to the d) occupancy of both T^+ and T^- tetrahedral environments which are above and below the plane of the anion net in monoclinic LSSI. This distinct Si_2S_7 dimer arrangement in triclinic $Li_7Si_2S_7I_{0.89}Cl_{0.11}$ generates alternating Si^{4+}-free and Si^{4+}-rich layers stacked along the *b* axis shown in e), compared to Si^{4+} environments that are f) evenly distributed within all layers along *b* in LSSI.

The distinct arrangements of Si_2S_7 dimers and the substitutionally disordered I^-/Cl^- site directs the Li^+ distribution in triclinic $Li_7Si_2S_7I_{0.89}Cl_{0.11}$ (Figure 2). Notably, triclinic $Li_7Si_2S_7I_{0.89}Cl_{0.11}$ has sixteen distinct Li^+ sites within the structure at 300 K, which is the same number as Ge^{4+}

View Article Online
DOI: 10.1039/D5SC09834C

substituted $Li_7Si_{0.88}Ge_{1.12}S_7I$ and one more than monoclinic LSSI at the same temperature. The site types occupied by Li^+ in all three materials are very similar (Figure 2), consisting of tetrahedral S_3X and octahedral S_3X_3, S_5X, and S_6 environments. There are, however, subtle differences between the three materials in the number of each occupied site type (Supporting Information, Table S6). Unlike $Li_7Si_{0.88}Ge_{1.12}S_7I$ in which the additional (sixteenth) Li^+ site occupies an S_6 octahedral environment within the hcp motif, the additional (sixteenth) site in $Li_7Si_2S_7I_{0.89}Cl_{0.11}$ resides within an S_5X environment in the sheared fcc-like motif. Thus, $Li_7Si_2S_7I_{0.89}Cl_{0.11}$ has the same number of occupied Li^+ sites in the hcp motif as monoclinic LSSI (eight) but one fewer than $Li_7Si_{0.88}Ge_{1.12}S_7I$ (nine), and one more Li^+ site (eight) occupied in the sheared fcc-like motif compared to both LSSI and $Li_7Si_{0.88}Ge_{1.12}S_7I$ (seven).

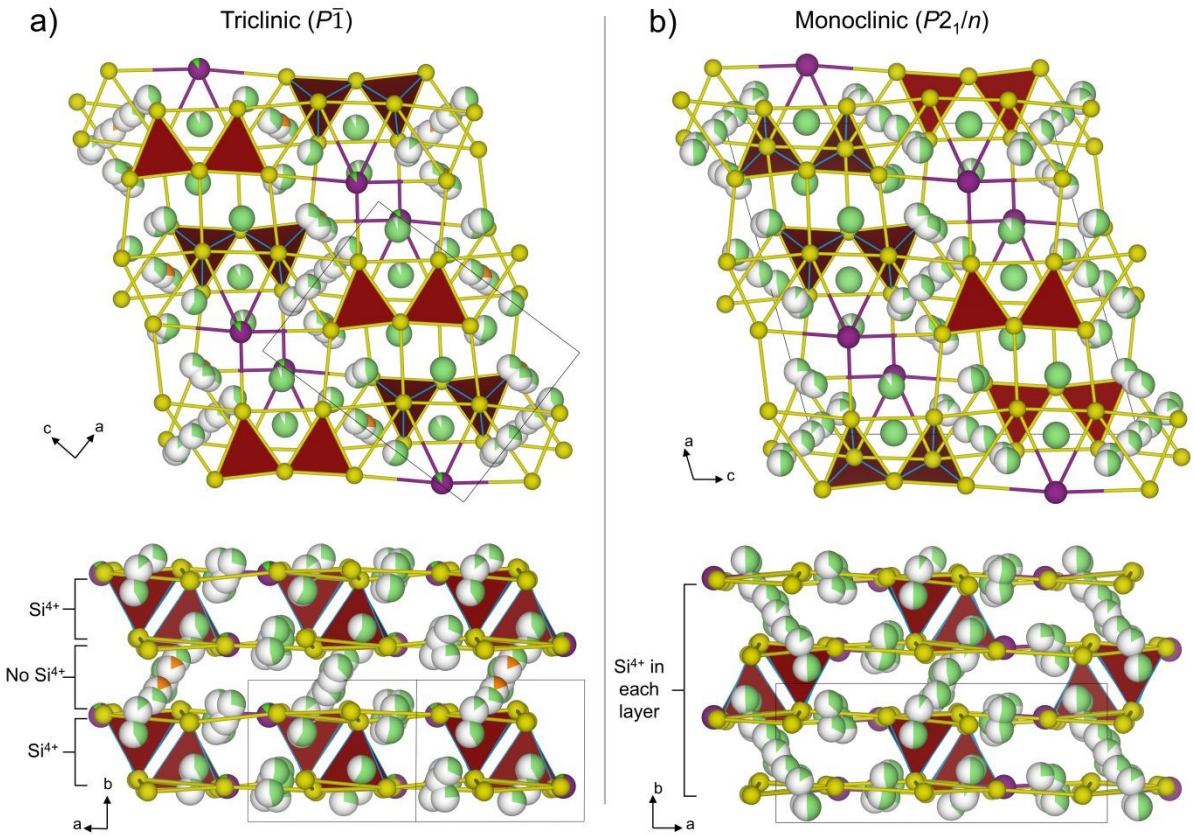

Figure 2. Crystal structures of a) triclinic $Li_7Si_2S_7I_{0.89}Cl_{0.11}$ and b) monoclinic LSSI at 300 K with lithium sites shown as partially occupied green spheres viewed along the *b* and *c* directions. The partially occupied orange spheres visible in a) represent the new Li^+ positions of triclinic $Li_7Si_2S_7I_{0.89}Cl_{0.11}$ distinct to those in monoclinic LSSI.

The exact Li^+ site distributions within the hcp and sheared fcc-like motifs of triclinic $Li_7Si_2S_7I_{0.89}Cl_{0.11}$ have slight differences from those of monoclinic LSSI, which are associated with changes in the volumes of certain cation coordination environments following the partial substitution of I^- for Cl^- (Tables S7 and S8).[22] Firstly, one of the partially occupied Li^+ sites observed in the hcp motif of monoclinic LSSI is unoccupied in $Li_7Si_2S_7I_{0.89}Cl_{0.11}$. The S_3I-defined tetrahedra is partially occupied by Li^+ in monoclinic LSSI, however it is unoccupied in triclinic $Li_7Si_2S_7I_{0.89}Cl_{0.11}$ (labelled as $T2a_{hcp}$-2 in Figure 3a and 3b) as a result of the tetrahedral volume

View Article Online
DOI: 10.1039/D5SC09834C

decreasing from 7.7049(18) Å^3 to 7.655(3) Å^3, respectively. Secondly, a new distinct Li$^+$ position is observed in the hcp motif of $Li_7Si_2S_7I_{0.89}Cl_{0.11}$ which is unoccupied in monoclinic LSSI. This site is located on a 1*b* Wyckoff position at the centre of an S_6 octahedron in the hcp motif (site shown in orange and labelled as $O1a_{hcp}$-2 in Figure 3a). Despite the volume of this octahedron decreasing slightly from 26.180(8) Å^3 in monoclinic LSSI to 25.926(12) Å^3 in triclinic $Li_7Si_2S_7I_{0.89}Cl_{0.11}$, the occupation of this new site in $Li_7Si_2S_7I_{0.89}Cl_{0.11}$ results from the redistribution of Li$^+$ from the now unoccupied neighbouring $T2a_{hcp}$-2 environment described above. Thirdly, the Li$^+$ site that occupies a 2*c* Wyckoff position in the other S_6 octahedron (labelled as $O1a_{hcp}$-1 in Figure 3a and 3b) of the hcp motif in monoclinic LSSI splits onto a 2*i* Wyckoff position in triclinic $Li_7Si_2S_7I_{0.89}Cl_{0.11}$ such that it coordinates to four S^{2-} anions (site shown in orange in Figure 3a). This is a result of the $O1a_{hcp}$-1 S_6 octahedron volume increasing from 26.565(8) Å^3 to 26.665(13) Å^3, respectively. Thus, aside from the unoccupied $T2a_{hcp}$-2 site, the Li$^+$ site distribution within the hcp motif of $Li_7Si_2S_7I_{0.89}Cl_{0.11}$ is more closely comparable to that seen in $Li_7Si_{0.88}Ge_{1.12}S_7I$ rather than LSSI. Finally, the second additional Li$^+$ site occupied in $Li_7Si_2S_7I_{0.89}Cl_{0.11}$ that is not occupied in LSSI or $Li_7Si_{0.88}Ge_{1.12}S_7I$ is located within the sheared fcc-like motif on a 2*i* Wyckoff position in an S_5X octahedron (labelled as $O2_{fcc}$ in Figure 3a). This is enabled by a volume expansion of the $O2_{fcc}$ octahedron from 30.184(5) Å^3 in monoclinic LSSI to 30.237(8) Å^3 in triclinic $Li_7Si_2S_7I_{0.89}Cl_{0.11}$. The volumes of the environments discussed above in monoclinic LSSI and triclinic $Li_7Si_2S_7I_{0.89}Cl_{0.11}$ are compared in Figure 3e. The majority of the Li$^+$ environments that incorporate the mixed I^-/Cl^- position in $Li_7Si_2S_7I_{0.89}Cl_{0.11}$ decrease in volume (Tables S7 and S8) relative to monoclinic LSSI as a result of the reduced average ionic radius of that I^-/Cl^- position. The occupancies of all Li$^+$ sites observed in triclinic $Li_7Si_2S_7I_{0.89}Cl_{0.11}$ at 300 K are summarized in Table S3.

View Article Online
DOI: 10.1039/D5SC09834C

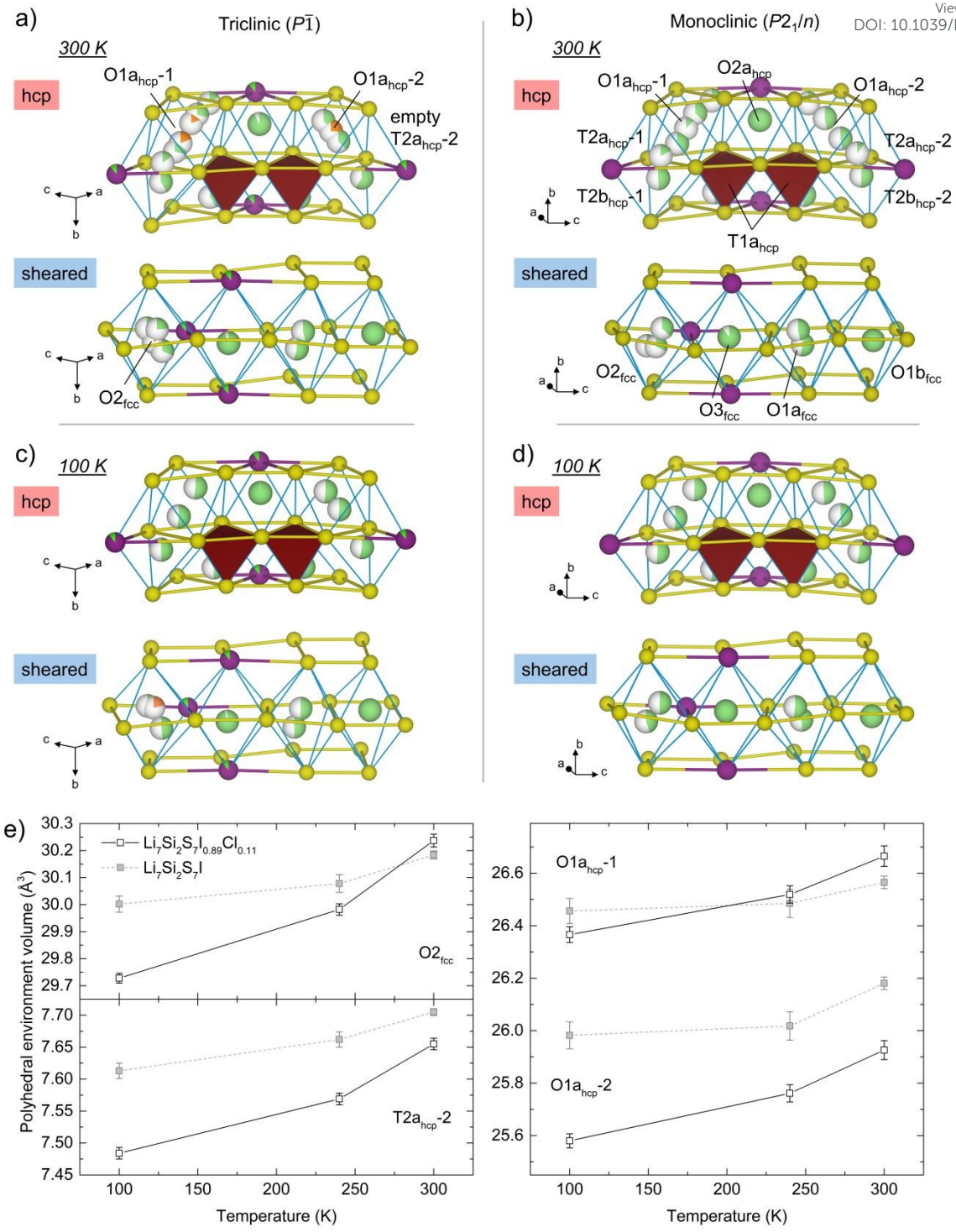

Figure 3. The Li^+ distribution in hcp and sheared fcc motifs of a, c) triclinic $Li_7Si_2S_7I_{0.89}Cl_{0.11}$ and b, d) monoclinic LSSI at 300 K and 100 K with lithium sites shown as partially occupied green spheres. The partially occupied orange spheres visible in a) and c) represent the new Li^+ positions in triclinic $Li_7Si_2S_7I_{0.89}Cl_{0.11}$ distinct from those observed in monoclinic LSSI. The tetrahedral void T2a$_{hcp}$-2, partially occupied by Li^+ in monoclinic LSSI, is unoccupied in triclinic $Li_7Si_2S_7I_{0.89}Cl_{0.11}$. Similar to monoclinic LSSI, triclinic $Li_7Si_2S_7I_{0.89}Cl_{0.11}$ undergoes an isostructural phase transition in which four of the sixteen Li^+ sites observed at 300 K become unoccupied at 100 K. The volumes of particular environments within monoclinic LSSI and triclinic $Li_7Si_2S_7I_{0.89}Cl_{0.11}$ as a function of temperature are compared in e).

View Article Online
DOI: 10.1039/D5SC09834C

Triclinic $Li_7Si_2S_7I_{0.89}Cl_{0.11}$ undergoes a similar isostructural phase transition to that observed in monoclinic LSSI with the depopulation of four Li^+ sites at low temperatures (Figure 3c and d). Two of the sixteen Li^+ sites occupied at 300 K in $Li_7Si_2S_7I_{0.89}Cl_{0.11}$ become unoccupied at 240 K (S_6-defined $O1a_{hcp}$-1 and S_3X-defined $T2a_{hcp}$-1), and a further two sites are unoccupied at 100 K (S_6-defined $O1a_{hcp}$-2 and S_5X-defined $O2_{fcc}$). Triclinic $Li_7Si_2S_7I_{0.89}Cl_{0.11}$ retains three Li^+ positions in the S_5X-defined $O2_{fcc}$ octahedron at 100 K (Figure 3c), which is one more than monoclinic LSSI at the same temperature (Figure 3d). Precise tuning of composition via volume-controlling substitution, such as the Ge^{4+} substitution for Si^{4+} demonstrated for monoclinic LSSI, may present a promising strategy for optimisation of the property-determining Li^+ distribution within the triclinic structure.

Though crystal growth of triclinic $Li_7Si_2S_7I_{0.89}Cl_{0.11}$ was successful, despite extensive efforts it was not possible to isolate a high purity powder sample preventing the experimental measurement of ionic conductivity, even with the compositional guidance provided by SEM-EDX. Triclinic $Li_7Si_2S_7I_{0.89}Cl_{0.11}$ was not observed in any bulk powder reactions that were performed at a range of different compositions and synthesis conditions (Table S1). In all cases, the monoclinic phase of LSSI was observed, and the phase purity decreased in both compositions with increased Cl content, or reactions run at higher synthesis temperatures (Figure S3). Thus, the synthesis of triclinic $Li_7Si_2S_7I_{0.89}Cl_{0.11}$ is more complicated than targeting a specific composition alone. We note that the exact crystal growth procedure in which triclinic $Li_7Si_2S_7I_{0.89}Cl_{0.11}$ is observed differs from the procedure used for monoclinic LSSI, which utilised elemental S as the flux, as well as different growth temperatures and durations. Indeed, crystals of triclinic $Li_7Si_2S_7I_{0.89}Cl_{0.11}$ were obtained only from the syntheses which utilised the 35%LiCl-65%LiI eutectic flux (Supporting Information); triclinic $Li_7Si_2S_7I_{0.89}Cl_{0.11}$ was not observed in any elemental S flux growths that yield monoclinic LSSI, or even $Li_7Si_{2-x}Ge_xS_7I$. This indicates that triclinic $Li_7Si_2S_7I_{0.89}Cl_{0.11}$ may be accessible only under a narrow range of synthesis conditions and that competition with monoclinic LSSI makes experimental isolation as a bulk powder challenging.

In the absence of experimental measurements of the conductivity, the Li^+ ion transport properties of triclinic $Li_7Si_2S_7I_{0.89}Cl_{0.11}$ were thus examined by *ab initio* molecular dynamics (AIMD) simulations[23-29] that used the experimentally determined crystal structure, where the framework-forming Si, S and halide sites that define the pathways within which the heavily disordered Li move are well-defined crystallographically: the MD simulations naturally account for the disorder in the highly mobile Li. These simulations demonstrated that the overall ion transport is highly comparable to that of monoclinic LSSI (Figure 4a-d). Specifically, the calculated diffusion coefficients along each crystallographic axis are comparable with those of LSSI and agree within a factor of two indicating 3D Li^+ mobility which results from the vast array of migration pathways provided by the structure (Figure 4f), as in LSSI. A theoretical activation energy of 0.16(4) eV is extracted for $Li_7Si_2S_7I_{0.89}Cl_{0.11}$ from the mean squared displacements across simulations at 400-500 K, and a computed bulk ionic conductivity of 0.019(7) S cm^{-1} extrapolated to 300 K (Figure 4e). These values are within error of those

View Article Online
DOI: 10.1039/D5SC09834C

obtained from equivalent AIMD simulations on monoclinic LSSI with an activation energy of 0.16(1) eV and calculated conductivity of 0.023(9) S cm^{-1}. These simulations further support that the intermetallic-derived anion framework of LSSI enables rapid Li^+ ion transport throughout the structure, and that the Li mobility pathways and associated computed high performance is retained despite changes to both the crystal system and arrangement of the framework-forming Si_2S_7 dimers.

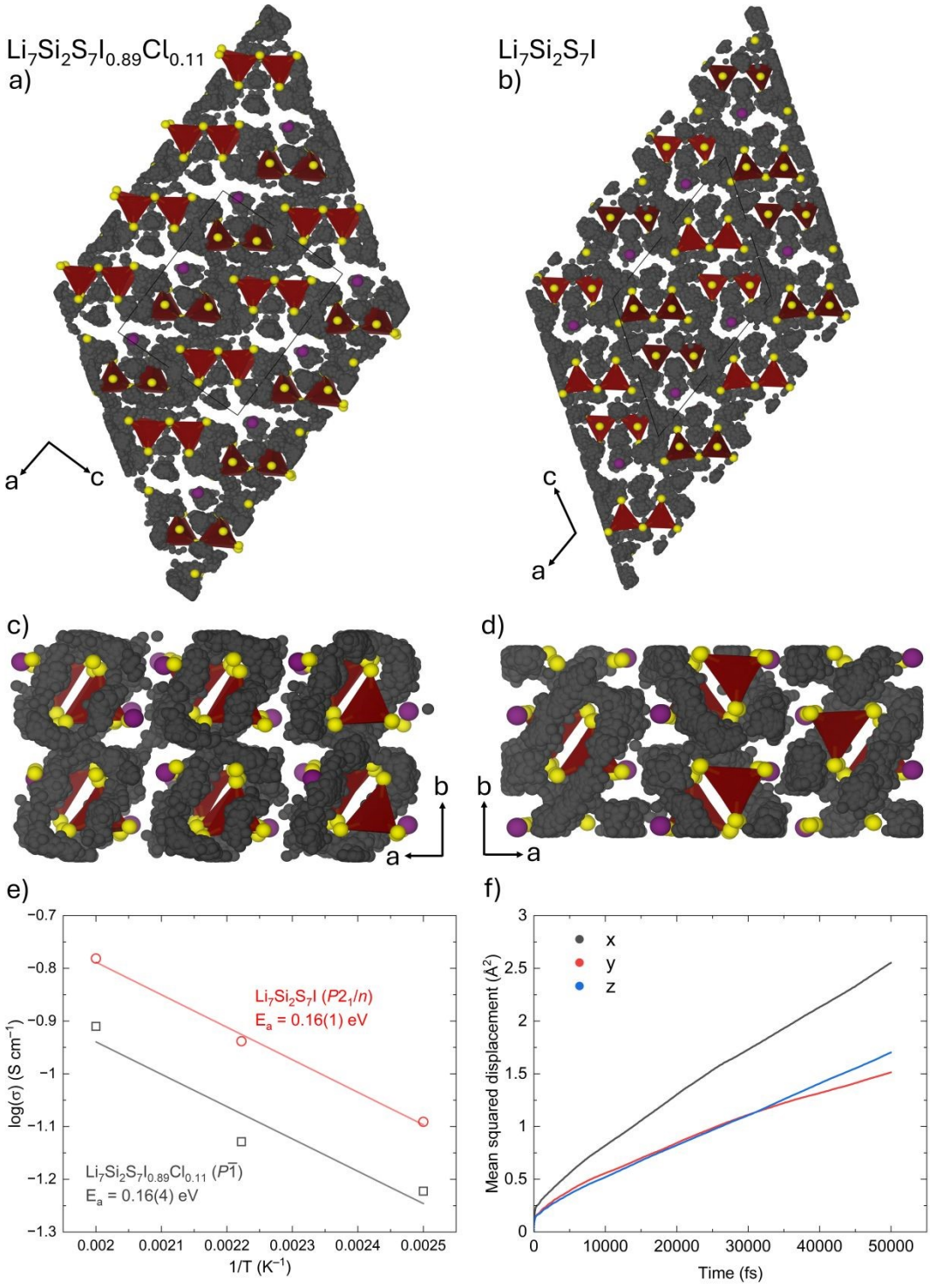

Figure 4. AIMD simulation of a) triclinic $Li_7Si_2S_7I_{0.89}Cl_{0.11}$ (model composition $Li_7Si_2S_7I$) and b) monoclinic LSSI. Black points indicate the calculated Li^+ positions taken at time intervals of 0.5 ps from the 250 ps AIMD simulation at 500 K for $Li_7Si_2S_7I_{0.89}Cl_{0.11}$, and 0.5 ps intervals from a 300 ps AIMD simulation at 500 K for LSSI.[16] Projections along *c* for c) $Li_7Si_2S_7I_{0.89}Cl_{0.11}$ and d) LSSI. e) Comparison of computed ionic conductivities (log(σ)) for $Li_7Si_2S_7I_{0.89}Cl_{0.11}$ and LSSI, with extracted activation energies. f) Mean squared displacements (msd) of the three crystallographic axes in $Li_7Si_2S_7I_{0.89}Cl_{0.11}$ at 500 K. Comparable gradients for all three traces indicate that $Li_7Si_2S_7I_{0.89}Cl_{0.11}$ is a 3D Li^+ ion conductor. Panel b) is reproduced or adapted with permission from Ref. 16. Copyright 2025 The American Association for the Advancement of Science.

Conclusions

$Li_7Si_2S_7I_{0.89}Cl_{0.11}$ is effectively a triclinic polymorph of LSSI. It demonstrates that the anion framework originally observed in $Li_7Si_2S_7I$, derived from the sphere packings within the NiZr intermetallic, can accommodate changes in both crystal system and the location of framework-forming Si^{4+} cations. The ordered arrangement of S^{2-} and X^- anions from LSSI is retained, while the substitution at the halide site generates distinct orientations of Si_2S_7 dimers that produce alternating arrangements of silicon-free and silicon-rich layers along the stacking axis. The ability to vary the orientation of Si_2S_7 dimers is an additional degree of freedom for the control of structure and properties beyond those of the argyrodite and LGPS families, whose structures are defined by isolated tetrahedral MS_4 positions. Triclinic $Li_7Si_2S_7I_{0.89}Cl_{0.11}$ has sixteen distinct Li^+ sites in total, one more than LSSI, and retains a superionic computed conductivity and low computed activation energy. Polymorphism is known to significantly impact ion transport in other Li^+ conductor families, e.g. the Li^+ site ordering observed in argyrodite and thio-LISICON materials.[30-34] The LSSI ordered S/halide anion framework maintains multiple low energy pathways from AIMD simulations for lithium motion despite significant changes in the framework-forming cation distribution associated with the reduction in symmetry from monoclinic to triclinic. This persistence of predicted high ion mobility from simulation in the presence of polymorphism suggests that there are privileged anion frameworks that can tolerate changes in cation distribution while retaining superionic transport.

Acknowledgements

The authors thank the Engineering and Physical Sciences Research Council (EPSRC) for funding under EP/V026887. We thank the Leverhulme Research Centre for Functional Materials Design for support to C.C. M.S. acknowledges financial support from the Faraday Institution CATMAT project (EP/S003053/1, FIRG016). We acknowledge Diamond Light Source for access to beamline I11 (CY37989). This work used the ARCHER2 UK National Supercomputing Service(https://www.archer2.ac.uk) with compute time allocated as part of EPSRC grant EP/V026887.

Author Contributions

View Article Online
DOI: 10.1039/D5SC09834C

GH developed synthetic methodology for isolation of the new phase. GH solved the crystal structure with support from CMR, LMD and JBC. CMC performed AIMD simulations to predict ion transport behaviour with support of MSD. MS conducted measurements for elemental analysis. MJR directed the research and acquired funding. GH and LMD composed the initial draft of the manuscript. All authors contributed to the review and editing of the manuscript.

Supporting Information

Additional data in figures and tables are available in the Supporting Information. The crystal structures of $Li_7Si_2S_7I_{0.89}Cl_{0.11}$ at a range of temperatures are deposited with CSD accession codes 2429627 (100 K), 2429628 (240 K), and 2429626 (300 K).

Data Availability

The data that support the findings of this research will be made openly available via the University of Liverpool open research platform Liverpool Elements on acceptance of the publication.

Conflicts of interest

The authors declare no conflicts of interest.

References

1 J. M. Tarascon and M. Armand, Issues and challenges facing rechargeable lithium batteries, *Nature,* 2001, **414**, 359-367. DOI: 10.1038/35104644.
2 B. Singh, Y. Wang, J. Liu, J. D. Bazak, A. Shyamsunder and L. F. Nazar, Critical Role of Framework Flexibility and Disorder in Driving High Ionic Conductivity in $LiNbOCl_4$, *J. Am. Chem. Soc.,* 2024, **146**, 17158-17169. DOI: 10.1021/jacs.4c03142.
3 K. Wang, Q. Ren, Z. Gu, C. Duan, J. Wang, F. Zhu, Y. Fu, J. Hao, J. Zhu, L. He, C.-W. Wang, Y. Lu, J. Ma and C. Ma, A cost-effective and humidity-tolerant chloride solid electrolyte for lithium batteries, *Nat. Commun.,* 2021, **12**, 4410. DOI: 10.1038/s41467-021-24697-2.
4 R. Chen, W. Qu, X. Guo, L. Li and F. Wu, The pursuit of solid-state electrolytes for lithium batteries: from comprehensive insight to emerging horizons, *Mater. Horiz.,* 2016, **3**, 487-516. DOI: 10.1039/C6MH00218H.
5 J. Janek and W. G. Zeier, Challenges in speeding up solid-state battery development, *Nat. Energy,* 2023, **8**, 230-240. DOI: 10.1038/s41560-023-01208-9.
6 Y. Kato, S. Hori and R. Kanno, $Li_{10}GeP_2S_{12}$-Type Superionic Conductors: Synthesis, Structure, and Ionic Transportation, *Adv. Energy Mater.,* 2020, **10**, 2002153. DOI: https://doi.org/10.1002/aenm.202002153.
7 Y. Wang, W. D. Richards, S. P. Ong, L. J. Miara, J. C. Kim, Y. Mo and G. Ceder, Design principles for solid-state lithium superionic conductors, *Nat. Mater.,* 2015, **14**, 1026-1031. DOI: 10.1038/nmat4369.

8 J. C. Bachman, S. Muy, A. Grimaud, H.-H. Chang, N. Pour, S. F. Lux, O. Paschos, F. Maglia, S. Lupart, P. Lamp, L. Giordano and Y. Shao-Horn, Inorganic solid-state electrolytes for lithium batteries: mechanisms and properties governing ion conduction, *Chem. Rev.,* 2016, **116**, 140-162. DOI: 10.1021/acs.chemrev.5b00563.
9 N. Kamaya, K. Homma, Y. Yamakawa, M. Hirayama, R. Kanno, M. Yonemura, T. Kamiyama, Y. Kato, S. Hama, K. Kawamoto and A. Mitsui, A lithium superionic conductor, *Nat. Mater.,* 2011, **10**, 682-686. DOI: 10.1038/nmat3066.
10 Y. Li, S. Song, H. Kim, K. Nomoto, H. Kim, X. Sun, S. Hori, K. Suzuki, N. Matsui, M. Hirayama, T. Mizoguchi, T. Saito, T. Kamiyama and R. Kanno, A lithium superionic conductor for millimeter-thick battery electrode, *Science,* 2023, **381**, 50-53. DOI: doi:10.1126/science.add7138.
11 Y. Kato, S. Hori, T. Saito, K. Suzuki, M. Hirayama, A. Mitsui, M. Yonemura, H. Iba and R. Kanno, High-power all-solid-state batteries using sulfide superionic conductors, *Nat. Energy,* 2016, **1**, 16030. DOI: 10.1038/nenergy.2016.30.
12 J. Zhou, P. Chen, W. Wang and X. Zhang, $Li_7P_3S_{11}$ electrolyte for all-solid-state lithium-ion batteries: structure, synthesis, and applications, *Chem. Eng. J.,* 2022, **446**, 137041. DOI: https://doi.org/10.1016/j.cej.2022.137041.
13 H. Yamane, M. Shibata, Y. Shimane, T. Junke, Y. Seino, S. Adams, K. Minami, A. Hayashi and M. Tatsumisago, Crystal structure of a superionic conductor, $Li_7P_3S_{11}$, *Solid State Ionics,* 2007, **178**, 1163-1167. DOI: https://doi.org/10.1016/j.ssi.2007.05.020.
14 H.-J. Deiseroth, S.-T. Kong, H. Eckert, J. Vannahme, C. Reiner, T. Zaiß and M. Schlosser, Li_6PS_5X: A Class of Crystalline Li-Rich Solids With an Unusually High Li^+ Mobility, *Angew. Chem. Int. Ed.,* 2008, **47**, 755-758. DOI: https://doi.org/10.1002/anie.200703900.
15 P. Adeli, J. D. Bazak, K. H. Park, I. Kochetkov, A. Huq, G. R. Goward and L. F. Nazar, Boosting solid-state diffusivity and conductivity in lithium superionic argyrodites by halide substitution, *Angew. Chem. Int. Ed.,* 2019, **58**, 8681-8686. DOI: https://doi.org/10.1002/anie.201814222.
16 G. Han, A. Vasylenko, L. M. Daniels, C. M. Collins, L. Corti, R. Chen, H. Niu, T. D. Manning, D. Antypov, M. S. Dyer, J. Lim, M. Zanella, M. Sonni, M. Bahri, H. Jo, Y. Dang, C. M. Robertson, F. Blanc, L. J. Hardwick, N. D. Browning, J. B. Claridge and M. J. Rosseinsky, Superionic lithium transport via multiple coordination environments defined by two-anion packing, *Science,* 2024, **383**, 739-745. DOI: doi:10.1126/science.adh5115.
17 G. Han, L. M. Daniels, A. Vasylenko, K. A. Morrison, L. Corti, C. M. Collins, H. Niu, R. Chen, C. M. Roberston, F. Blanc, M. S. Dyer, J. B. Claridge and M. J. Rosseinsky, Enhancement of Low Temperature Superionic Conductivity by Suppression of Li Site Ordering in $Li_7Si_{2-x}Ge_xS_7I$, *Angew. Chem. Int. Ed.,* 2024, **63**, e202409372. DOI: https://doi.org/10.1002/anie.202409372.
18 X. Feng, P.-H. Chien, Y. Wang, S. Patel, P. Wang, H. Liu, M. Immediato-Scuotto and Y.-Y. Hu, Enhanced ion conduction by enforcing structural disorder in Li-deficient argyrodites $Li_{6-x}PS_{5-x}Cl_{1+x}$, *Energy Storage Materials,* 2020, **30**, 67-73. DOI: https://doi.org/10.1016/j.ensm.2020.04.042.
19 A. Gautam, H. Al-Kutubi, T. Famprikis, S. Ganapathy and M. Wagemaker, Exploring the Relationship Between Halide Substitution, Structural Disorder, and Lithium Distribution in Lithium Argyrodites ($Li_{6-x}PS_{5-x}Br_{1+x}$), *Chem. Mater.,* 2023, **35**, 8081-8091. DOI: 10.1021/acs.chemmater.3c01525.
20 S. V. Patel, S. Banerjee, H. Liu, P. Wang, P.-H. Chien, X. Feng, J. Liu, S. P. Ong and Y.-Y. Hu, Tunable Lithium-Ion Transport in Mixed-Halide Argyrodites $Li_{6-x}PS_{5-x}ClBr_x$: An Unusual

View Article Online
DOI: 10.1039/D5SC09834C

Compositional Space, *Chem. Mater.,* 2021, **33**, 1435-1443. DOI: 10.1021/acs.chemmater.0c04650.
21 L. Zhou, A. Assoud, Q. Zhang, X. Wu and L. F. Nazar, New Family of Argyrodite Thioantimonate Lithium Superionic Conductors, *J. Am. Chem. Soc.,* 2019, **141**, 19002-19013. DOI: 10.1021/jacs.9b08357.
22 R. J. Angel, M. L. Mazzucchelli, L. Baratelli, C. F. Schweinle, T. Balić-Žunić, J. Gonzalez-Platas and M. Alvaro, Uncertainties of recalculated bond lengths, angles and polyhedral volumes as implemented in the Crystal Palace program for parametric crystal structure analysis, *Acta Crystallogr., Sect. A:Found. Adv.,* 2025, **81**, 202-210. DOI: doi:10.1107/S2053273325002682.
23 S. Adams and R. Prasada Rao, Structural requirements for fast lithium ion migration in $Li_{10}GeP_2S_{12}$, *J. Mater. Chem.,* 2012, **22**, 7687-7691. DOI: 10.1039/C2JM16688G.
24 A. Baktash, J. C. Reid, T. Roman and D. J. Searles, Diffusion of lithium ions in Lithium-argyrodite solid-state electrolytes, *npj Comput. Mater.,* 2020, **6**, 162. DOI: 10.1038/s41524-020-00432-1.
25 J. A. Dawson and M. S. Islam, A Nanoscale Design Approach for Enhancing the Li-Ion Conductivity of the $Li_{10}GeP_2S_{12}$ Solid Electrolyte, *ACS Mater. Lett.,* 2022, **4**, 424-431. DOI: 10.1021/acsmaterialslett.1c00766.
26 N. J. J. de Klerk, I. Rosłoń and M. Wagemaker, Diffusion Mechanism of Li Argyrodite Solid Electrolytes for Li-Ion Batteries and Prediction of Optimized Halogen Doping: The Effect of Li Vacancies, Halogens, and Halogen Disorder, *Chem. Mater.,* 2016, **28**, 7955-7963. DOI: 10.1021/acs.chemmater.6b03630.
27 A. Gautam, M. Sadowski, N. Prinz, H. Eickhoff, N. Minafra, M. Ghidiu, S. P. Culver, K. Albe, T. F. Fässler, M. Zobel and W. G. Zeier, Rapid Crystallization and Kinetic Freezing of Site-Disorder in the Lithium Superionic Argyrodite Li_6PS_5Br, *Chem. Mater.,* 2019, **31**, 10178-10185. DOI: 10.1021/acs.chemmater.9b03852.
28 Y. Mo, S. P. Ong and G. Ceder, First Principles Study of the $Li_{10}GeP_2S_{12}$ Lithium Super Ionic Conductor Material, *Chem. Mater.,* 2012, **24**, 15-17. DOI: 10.1021/cm203303y.
29 B. J. Morgan, Mechanistic Origin of Superionic Lithium Diffusion in Anion-Disordered Li_6PS_5X Argyrodites, *Chem. Mater.,* 2021, **33**, 2004-2018. DOI: 10.1021/acs.chemmater.0c03738.
30 H.-J. Deiseroth, J. Maier, K. Weichert, V. Nickel, S.-T. Kong and C. Reiner, Li_7PS_6 and Li_6PS_5X (X: Cl, Br, I): Possible Three-dimensional Diffusion Pathways for Lithium Ions and Temperature Dependence of the Ionic Conductivity by Impedance Measurements, *Z. Anorg. Allg. Chem.,* 2011, **637**, 1287-1294. DOI: https://doi.org/10.1002/zaac.201100158.
31 S.-T. Kong, H.-J. Deiseroth, C. Reiner, Ö. Gün, E. Neumann, C. Ritter and D. Zahn, Lithium Argyrodites with Phosphorus and Arsenic: Order and Disorder of Lithium Atoms, Crystal Chemistry, and Phase Transitions, *Chem. - Eur. J.,* 2010, **16**, 2198-2206. DOI: https://doi.org/10.1002/chem.200902470.
32 S. T. Kong, Ö. Gün, B. Koch, H. J. Deiseroth, H. Eckert and C. Reiner, Structural Characterisation of the Li Argyrodites Li_7PS_6 and Li_7PSe_6 and their Solid Solutions: Quantification of Site Preferences by MAS-NMR Spectroscopy, *Chem. - Eur. J.,* 2010, **16**, 5138-5147. DOI: https://doi.org/10.1002/chem.200903023.
33 B. T. Leube, C. M. Collins, L. M. Daniels, B. B. Duff, Y. Dang, R. Chen, M. W. Gaultois, T. D. Manning, F. Blanc, M. S. Dyer, J. B. Claridge and M. J. Rosseinsky, Cation Disorder and Large Tetragonal Supercell Ordering in the Li-Rich Argyrodite $Li_7Zn_{0.5}SiS_6$, *Chem. Mater.,* 2022, **34**, 4073-4087. DOI: 10.1021/acs.chemmater.2c00320.

34 N. Minafra, S. P. Culver, C. Li, A. Senyshyn and W. G. Zeier, Influence of the Lithium Substructure on the Diffusion Pathways and Transport Properties of the Thio-LISICON $Li_4Ge_{1-x}Sn_xS_4$, *Chem. Mater.,* 2019, **31**, 3794-3802. DOI: 10.1021/acs.chemmater.9b01059.

View Article Online
DOI: 10.1039/D5SC09834C

The data that support the findings of this research will be made openly available via the University of Liverpool open research platform Liverpool Elements on acceptance of the publication.